Available online at www.sciencedirect.com
SCIENCE DIRECT®
PERGAMON
International Journal of Heat and Mass Transfer 46 (2003) 2841–2856
International Journal of HEAT and MASS TRANSFER
www.elsevier.com/locate/ijhmt

Heat transfer enhancement in cross-flow heat exchangers using oval tubes and multiple delta winglets

S. Tiwari, D. Maurya, G. Biswas *, V. Eswaran

Department of Mechanical Engineering, Indian Institute of Technology, Kanpur 208016, India

Received 16 July 2002; received in revised form 31 December 2002

Abstract

A three-dimensional study of laminar flow and heat transfer in a channel with built-in oval tube and delta winglets is carried out through the solution of the complete Navier–Stokes and energy equations using a body-fitted grid and a finite-volume method. The geometrical configuration represents an element of a gas–liquid fin–tube cross-flow heat exchanger. The size of such heat exchangers can be reduced through enhancement of transport coefficients on the air (gas) side, which are usually small compared to the liquid side. In a suggested strategy, oval tubes are used in place of circular tubes, and delta-winglet type vortex generators in various configurations are mounted on the fin-surface. An evaluation of the strategy is attempted in this investigation. The investigation is carried out for different angles of attack of the winglets to the incoming flow for the case of two winglet pairs. The variation of axial location of the winglets is also considered for one pair of winglets mounted in common-flow-down configuration. The structures of the velocity field and the heat transfer characteristics have been presented. The results indicate that vortex generators in conjunction with the oval tube show definite promise for the improvement of fin–tube heat exchangers.

1. Introduction

Fin–tubes (Fig. 1) are commonly used in many gas–liquid cross-flow heat exchangers. The fins are a series of thin parallel plates through which the tubes pass perpendicularly. In such an arrangement, the gas stream generally flows between the plates and across the tubes and the liquid flows inside the tubes. The fins act as extended surfaces providing the bulk of the heat transfer surface area for the gas side. Even with the extended surfaces, the dominant thermal resistance is on the side of the gas. In order to achieve significant heat transfer enhancement on the gas side, strategies must be developed to increase heat transfer coefficients on the fins and the tube outer surfaces without a large increase in pressure drop in the flow passage. The numerical investigations of Biswas et al. [1] and the experimental findings of Valencia et al. [2] reveal that effective utilization of vortex generators results in an enhancement of heat transfer without a significant additional penalty in the pressure drop.

In the above investigations, the enhancement of heat transfer from the fin surfaces is achieved by placing delta-winglet type vortex generators on the flat fin surfaces in the neighborhood of the tubes. Longitudinal vortices develop along the side-edge of the delta-winglets due to the pressure difference between the front surface (facing the flow) and the back surface. The longitudinal vortices (also called streamwise vortices) have axes aligned in the direction of the main flow. These vortices interact with an otherwise two-dimensional boundary layer and produce a three-dimensional swirling flow that mixes near-wall fluid with the mid-stream. This enhances the mixing of fluid from the periphery and the core regions of the flow field. Thus the thermal boundary layer is disrupted and heat transfer is enhanced. The additional pressure losses are modest because the form drag for such winglet-type slender bodies is low.

* Corresponding author. Tel.: +91-512-597616; fax: +91-512-597408.
E-mail address: gtm@iitk.ac.in (G. Biswas).

0017-9310/03/$ - see front matter © 2003 Elsevier Science Ltd. All rights reserved.
doi:10.1016/S0017-9310(03)00047-4

Nomenclature

a	semi-major diameter
b	semi-minor diameter
B	channel width
CV	control volume
BR	blockage ratio ($= 2b/B$)
F	mass flux through a cell face
H	channel height
k	thermal conductivity of the fluid
Nu	local Nusselt number based on bulk temperature, $(1/(1-\theta_b))\{\partial\theta/\partial Z\}_{Z=0}$
Nu_m	global Nusselt number
$\overline{Nu}_s$	span-wise averaged Nusselt number, $\int_0^B Nu\,dY/\int_0^B dY$
P	non-dimensional static pressure, $p/(\rho U_\infty^2)$
p	static pressure
Re	Reynolds number based on channel height $\rho U_\infty H/\mu$
S	surface area of a cell face
t	time
u	axial velocity
v	transverse velocity
w	normal or vertical velocity
x	axial dimension of coordinates
y	spanwise dimension of coordinates
z	normal or vertical dimension of coordinates
T	temperature

Greek symbols

ρ	density of the fluid
β	angle of attack
ξ	the curvilinear grid direction on the physical domain
η	the curvilinear grid direction on the physical domain perpendicular to the ξ = constant lines

Subscripts

av	average over the cross-section
b	bulk condition
i	cell center
j	cell face
w	wall
∞	condition at the entrance of the duct

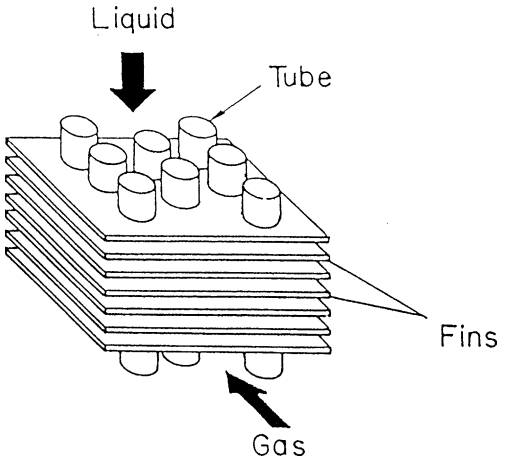

Fig. 1. Schematic representation of core region of a fin–tube heat exchanger.

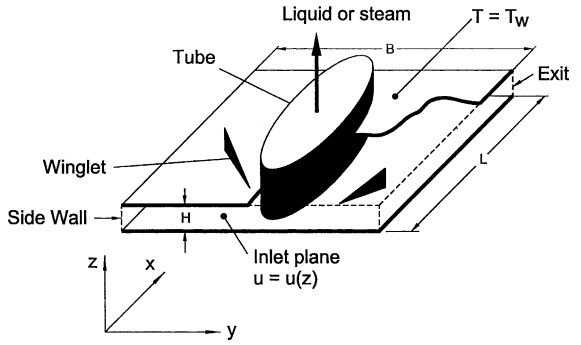

Fig. 2. Heat exchanger module with oval tube and vortex generators.

In order to study the improvement of the heat exchanger surfaces, the present numerical study investigates the use of oval tubes in place of circular tubes, with delta-winglets mounted in front of the oval tubes [3]. Vortex generators can be mounted in the fin–tube heat exchangers using following two common configurations, (i) common-flow-down and (ii) common-flow-up, as proposed by Pauley and Eaton [4]. Fig. 2 presents a sectional view of the suggested arrangement with the delta-winglets placed in a common-flow-down configuration in front of the oval tube. It may be mentioned that the study of low Reynolds number simulations in the present work is not for computational simplification. Usually, the fin spacing is so small and the mean velocity range is such that the flows are often laminar and the Reynolds numbers in the passages are in the range of low and moderate [5]. The complete Navier–Stokes equations together with the energy equation have been solved to obtain a detailed analysis of the flow structure together with heat transfer characteristics of the proposed configuration for the finned oval tube heat exchangers.

2. Mathematical formulation

The plan-view representation of the computational domain is shown in Fig. 3. The dimensions used are those of a proposed design being reported elsewhere by the authors. Two neighboring fins form a channel of height H, width $B = 11.25H$ and length $L = 13.75H$. The built-in oval tube, of semi-major diameter $a = 4.40H$ and semi-minor diameter $b = 1.465H$, is located at a distance $L1 = 6.87H$ from inlet of the channel. The tube center is located at $X = 6.87H$, $Y = 5.625H$.

The winglets are thin triangular devices (shown on top right of Fig. 3) placed vertically on the fin surface, with their horizontal axis from the tip either angled outward or inward from the centerline. The position of the winglets is shown as W1 and W2. If it is angled outward (see W1 in Fig. 3), it is called common-flow-down (CFD) configuration and if angled inwards (W2 in same figure), it is the common-flow-up (CFU) configuration. The axial distance (X11) between the leading edge of the first winglet pair in common-flow-down configuration and the channel inlet is $1.63H$. The transverse distance (Y11) between the channel centerline and the leading edge of either winglet is $2.23H$. The axial distance (X12) between the trailing edge of the either winglet and the channel inlet is $3.38H$. The transverse distance (Y12) between the channel centerline and the trailing edge of either winglet is $3.69H$. The other winglet of the first winglet pair is placed symmetrically about the channel centerline. The axial distance (X21) of the leading edge of second pair of winglets in common-flow-up configuration from the inlet of channel is $3.96H$ and transverse distance (Y21) from the centerline of the channel is $5.33H$. The axial distance (X22) between trailing edge of the second pair of winglet and channel inlet is $5.71H$ and the distance (Y22) of it from the channel centerline is $3.88H$. The length of all the winglets is $2.27H$ and their height is $h = 0.5H$. Fig. 4 shows a layout of various configurations in which winglet pairs are mounted in the present study. Computations are performed for each of these configurations. Air has been considered as the working fluid, hence the Prandtl number is taken as 0.7. The winglets and oval tube are assumed to be at the temperature of the channel wall.

3. Governing equations

The three-dimensional continuity, Navier–Stokes and energy equations for laminar flow are:

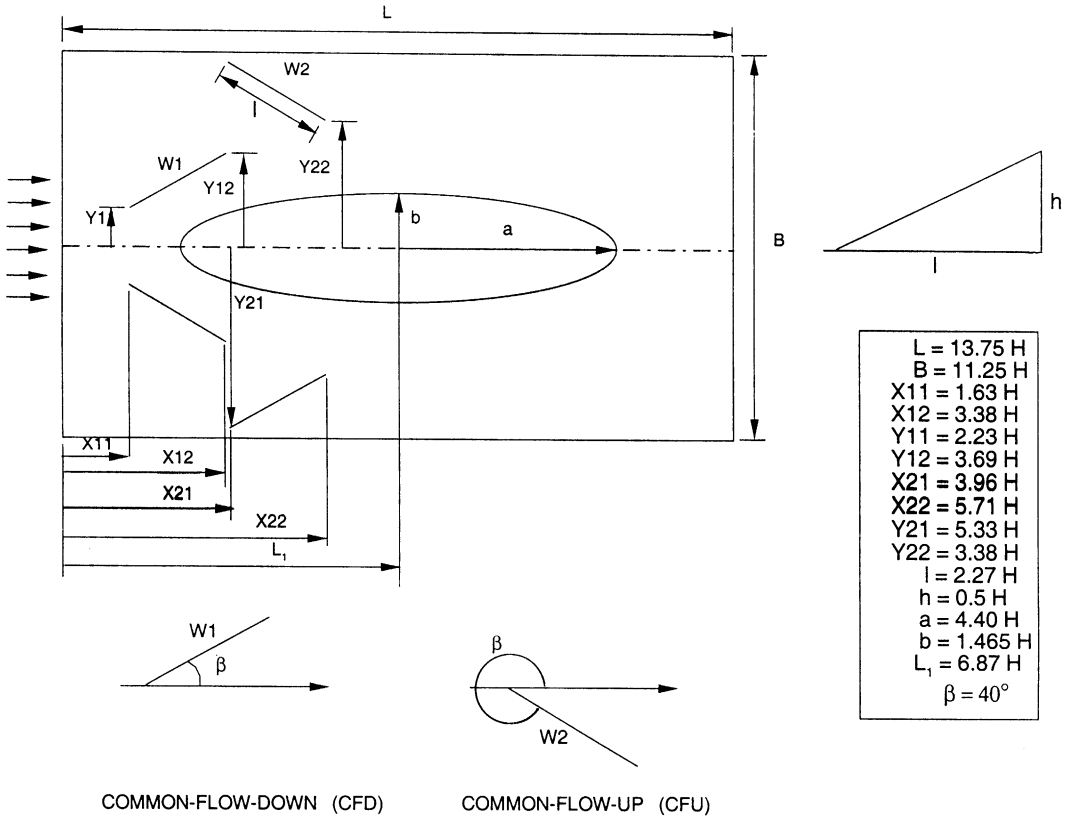

Fig. 3. Two-dimensional representation of the computational domain.

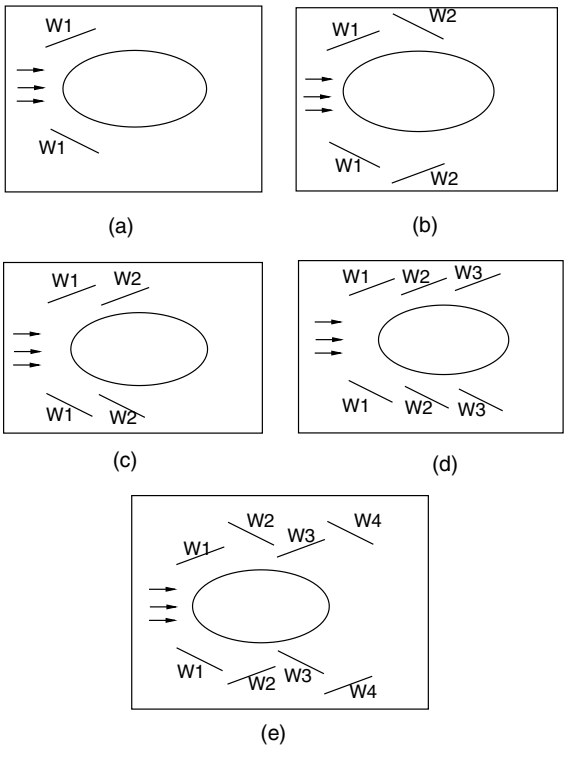

Fig. 4. Various configurations of the winglet pairs. (a) One winglet pair (W1) in CFD. (b) Two winglet pairs (W1 in CFD and W2 in CFU). (c) Two winglet pairs (W1 and W2 both in CFD). (d) Three winglet pairs (W1, W2 and W3 in CFD). (e) Four winglet pairs (W1 and W3 in CFD; W2 and W4 in CFU).

$$\frac{\partial u_i}{\partial x_i} = 0 \tag{1}$$

$$\frac{\partial u_i}{\partial t} + u_j \frac{\partial u_i}{\partial x_j} = -\frac{1}{\rho}\frac{\partial p}{\partial x_i} + v\frac{\partial^2 u_i}{\partial x_j \partial x_j} \tag{2}$$

$$\frac{\partial T}{\partial t} + u_j \frac{\partial T}{\partial x_i} = \alpha \frac{\partial^2 u_i}{\partial x_j \partial x_j} \tag{3}$$

4. Boundary conditions

The boundary conditions used in the present investigation are:

- Top and bottom plates
  $u = v = w = 0$ (no slip boundary condition) and $\partial p/\partial z = 0$
  $T = T_w$ (T_w represents wall temperature)
- Side wall $\partial u/\partial y = \partial w/\partial y = 0$, $v = 0$ (free slip boundary condition) and $\partial p/\partial y = 0$, $\partial T/\partial y = 0$
- Channel inlet $u = U_\infty$, $v = w = 0$ and $\partial p/\partial x = 0$
  $T = T_\infty$ (fluid temperature at the inlet)
- Channel exit: The mass flux through the outlet boundaries is found by means of a continuative outflow condition [6], which allows changes inside the flow field to be transmitted outward, but not vice-versa. This boundary condition uses an upwinded form of the following equation for each velocity component and temperature
  $(\partial\phi/\partial t) + U_{av}(\partial\phi/\partial x) = 0$ (where ϕ represents u, v, w or T).
  The pressure is also specified at the outflow:
  $p = p_{exit}$ (atmospheric pressure)
- Obstacles: Oval tube and the winglet pair
  $u = v = w = 0$ and $\partial p/\partial n = 0$ (where n signifies the normal direction to the surface) and $T = T_w$.

5. Grid generation

Fig. 5 shows a schematic representation of the two-dimensional grid employed in the present computation. The grid is generated using a block-partitioning method. The whole computational domain is divided into two blocks. In the first block where winglets are mounted on the fin-surface, a Cartesian grid is used, while in the other block the oval tube is placed. In this block, around the oval tube, a two-dimensional body-fitted grid is generated by transfinite interpolation. This is basically an algebraic method of generating the body-fitted grid. In this method, first the two extreme boundaries are matched with same number of points on them, and then the interior grid lines are obtained by interpolation. The grid is further smoothened by the use of elliptic partial differential equations. The technique of locating coordinates of the nodes on the domain boundary is called transfinite interpolation, if the ξ-constant and η-constant lines within the physical space, upon transformation, become equi-spaced orthogonal grid lines inside a rectangular domain of size 1×1. To generate the three-dimensional grid, the two-dimensional grid-mesh is replicated in the z-direction with uniform spacing.

6. Finite volume method

A finite-volume method due to Eswaran and Prakash [7] has been used to discretize and solve the governing conservation equations. The procedure of Eswaran and Prakash [7] has been documented in the recent work of Prabhakar et al. [8].

7. Results and discussion

A $62 \times 61 \times 19$ three-dimensional grid-mesh is used for the numerical study of flow and heat transfer in a

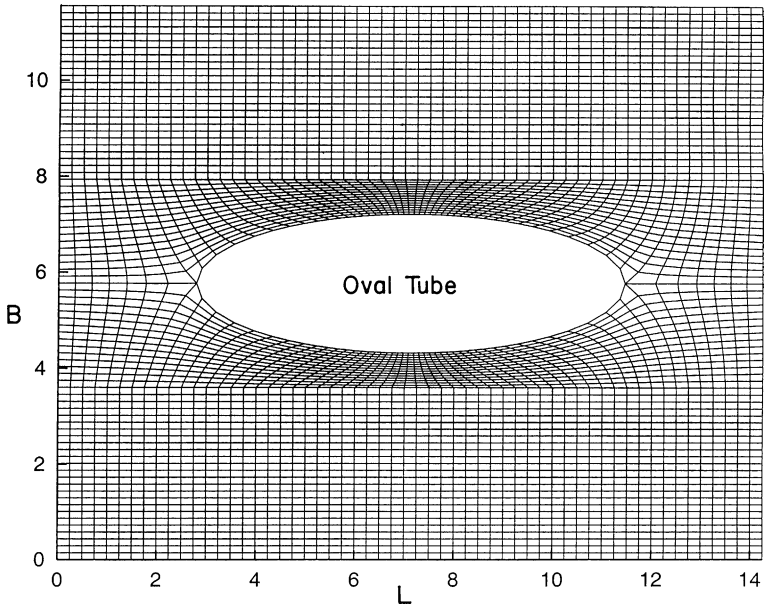

Fig. 5. The schematic of the grid-system on a two-dimensional plane.

channel with built-in oval tube and delta-winglet type vortex generators in common-flow-down (W1) and common-flow-up (W2) configurations as shown in Fig. 3. The present computations are carried out for various configurations of the winglet pairs as shown in Fig. 4. In the configuration of Fig. 4(a), different axial positions of one delta winglet pair are considered for an angle of attack of 40°. For the configuration of Fig. 4(b), the investigations are carried out for three different angles of attack of 30°, 35° and 40°. The blockage ratio (of the minor diameter of oval tube to the width of channel) is 0.26. The Reynolds number in the present study is 1000, based on the incoming average fluid velocity and the channel height. The span-averaged Nusselt number ($\overline{Nu_s}$), based on the bulk-mean temperature, has been used for comparing the heat transfer performance. The delta-winglets are taken to be non-conductors of heat and so conjugate heat transfer analysis is not required in our present problem. Considering a possible practical scenario, the winglets are likely to be punched out from the fins. Therefore, creation of a winglet can result in a punched hole on the fin and the winglet being of the same material as that of the fin, will be a conductor. The cumulative effect of these two variations may not be trivial. However, we have assumed the winglets to be the non-conductors in this study and focussed primarily on the transport enhancement due to the swirling motion.

We briefly discuss the preferability of oval tubes against circular tubes. Fig. 6(a) and (b) show the streamline plots at the mid-plane of the channel, corresponding to the instantaneous field, for flow past a built-in circular tube and an oval tube (both with the same cross-sectional perimeter) placed in a channel. The flow past the circular tube, clearly exhibits the phenomenon of vortex shedding (Fig. 6(a)), which not seen in the second case of flow past the oval tube (Fig. 6(b)). Such a distinguishing behavior can be attributed to the streamlined nature of the oval tube. The streamline plot for the time-averaged flow at the mid-plane of the channel, shown in Fig. 6(c), is seen to be nearly identical to that of the instantaneous field as already shown in Fig. 6(b). Thus the flow past an oval tube gives rise to a steady state solution unlike the time-periodic dynamic steady state response shown by a circular tube. This lack of vortex shedding lowers the inlet–exit pressure drop for the oval tube case, adding to its advantages. In all the results that follow, corresponding to various configurations of the vortex generators, the heat transfer analysis is carried out using the time-averaged flow.

Fig. 7(a) shows the limiting streamlines for the time-averaged flow, in the region close to the bottom plate, corresponding to the initially proposed problem. The incoming flow does not separate in the usual manner (of circular tubes) but reaches a stagnation or saddle point of separation (marked A). The nodal point of attachment or stagnation line is marked B in the figure. The separation lines form elliptical arcs along the tube. The point C indicates where horseshoe vortices graze the channel walls in the time-averaged flow field. These horseshoe vortices are formed in the region between B and C, at the top and bottom walls of the channel. Fig. 7(b) shows the local Nusselt number distribution on the

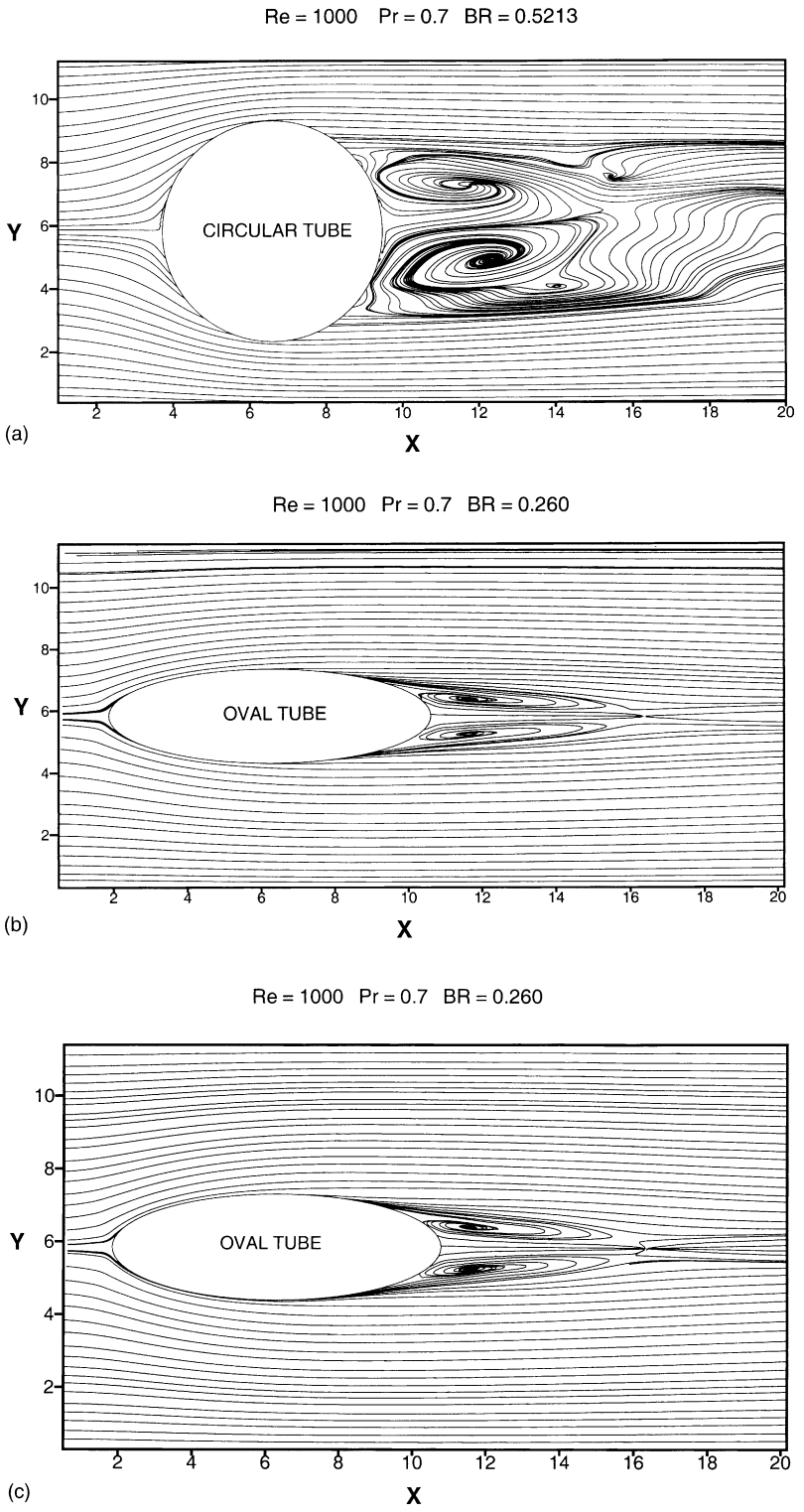

Fig. 6. (a) Streamline plot of the instantaneous field at the mid-plane shows vortex shedding (circular tube without winglets). (b) Streamline plot of the instantaneous field at the mid-plane (oval tube without winglets and having same perimeter as the circular tube). (c) Streamline plot of the time-averaged field at the mid-plane (oval tube without winglets).

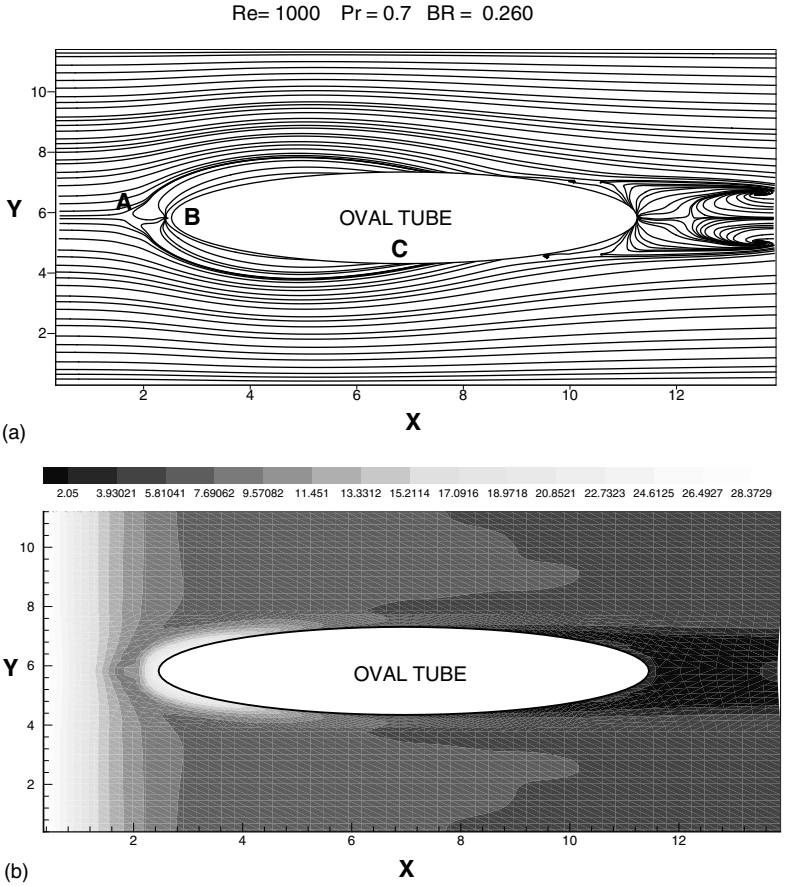

Fig. 7. (a) Streamline plot of the time-averaged field on the bottom plate (oval tube without winglets). (b) Iso-Nusselt number distribution on the bottom plate (oval tube without winglets).

bottom wall of the channel. At the leading edge of the channel, cool incoming fluid comes in contact with the fin surface for the first time, so the local Nusselt number is high everywhere near the leading edge. The gradual decrease in Nusselt number away from the leading edge is due to the growth of the boundary layer on the channel walls. However, an abrupt increase in Nusselt number in front of the oval tube is observed. This is due to the swirling action of the horseshoe vortices, which brings about a better mixing due to which the heat transfer in the neighborhood is enhanced significantly. The Nusselt number is again low in the wake region as shown in the figure. This is due to separated dead water zone with low re-circulating fluid velocity.

Fig. 8(a) shows limiting streamlines on a plane close to the bottom plate for the flow through rectangular channel with built-in oval tube and one pair of winglets in common-flow-down (W1) configuration (i.e. the other pair, W2, in Fig. 3 is removed). This geometry is for the configuration shown in Fig. 4(a). The winglets generate longitudinal vortices in the downstream. The saddle point of separation and the nodal point of attachment are visible in the figure. The time-averaged wake is symmetric. The twisted streamlines, near the winglets are the footprints of the swirling motion in the x–y plane, which has a dominant component in the transverse direction. The transverse momentum transfer to the near field boundary layer of the aft region of the oval tube delays the separation. Fig. 8(b) shows the distribution of local Nusselt number on the bottom plate of the channel corresponding to the flow field of Fig. 8(a). At the leading edge of the channel and near the oval tube, the local Nusselt number distribution has the same upward trend as in the earlier case for the reasons explained before. The heat transfer enhancement associated with the winglet pair in this case is evident in the figure. In the downstream region of each winglet pair, a strong influence of the swirling motion exists and its effect persists over a non-dimensional distance of 8 (eight). The heat transfer enhancement due to the corner (horseshoe) vortex of each winglet appears as a streak in the figure that begins on the upstream side of

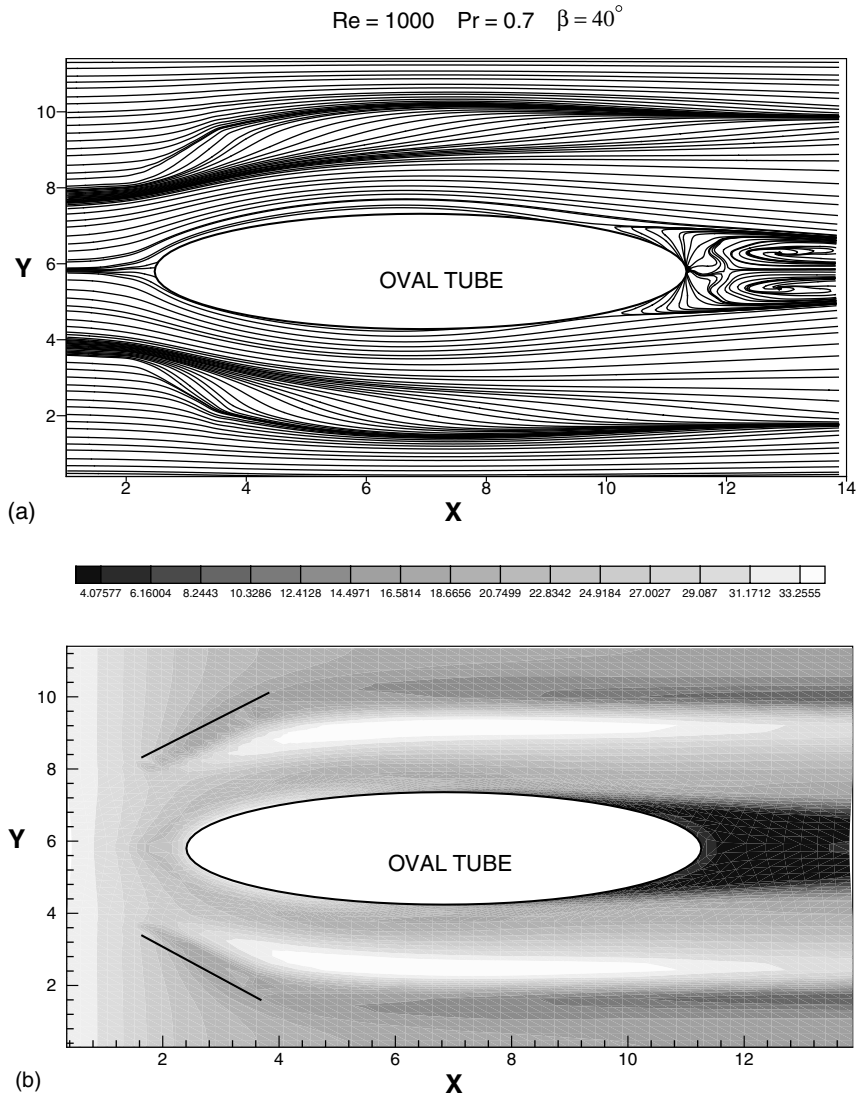

Fig. 8. (a) Limiting streamlines on the bottom plate for flow past a built-in oval tube with one pair of winglets. (b) Iso-Nusselt number distribution on the bottom plate for flow past a built-in oval tube with one winglet pair.

the winglet and is swept downstream wrapping the winglet.

Fig. 9 shows the iso-Nusselt number distribution on the bottom plate of the channel for the above-mentioned configuration (Fig. 4(b)) of two winglet pairs. Local regions of high heat transfer associated with the tube stagnation region, the horseshoe vortex system due to the tube, and the main (primary) and corner (horseshoe) vortices produced by each winglet are visible in the figure. In this context, it is worth mentioning that the horseshoe or necklace vortices are created due to variation in total pressure along the stagnation line on the pressure surface of the winglet [9]. The smaller velocity in the boundary layer on the flat bottom wall which is attached to the side of the winglet leads to a smaller pressure increase on the stagnation line. Thus the induced pressure gradient on the stagnation line causes a flow towards the bottom wall which interacts with the mainstream. The fluid rolls up forming vortices looking like a half horseshoe.

Fig. 10 shows the iso-Nusselt number distribution on the bottom plate of the channel for the parallel configuration of two winglet pairs (both W1 and W2 in common-flow-down configuration as in Fig. 4(c)). The local regions of high heat transfer associated with the above-mentioned attributes can be seen to be modified

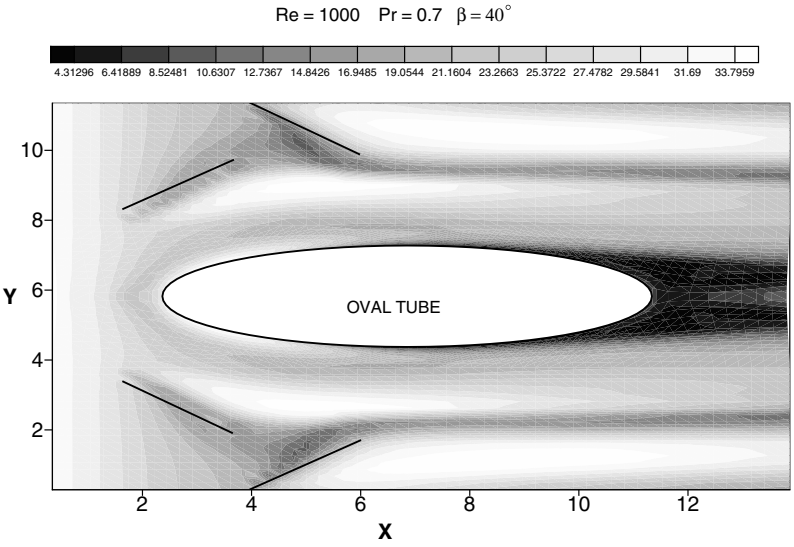

Fig. 9. Iso-Nusselt number distribution on the bottom plate for flow past a built-in oval tube with two winglet pairs (the configuration shown in Fig. 4(b)).

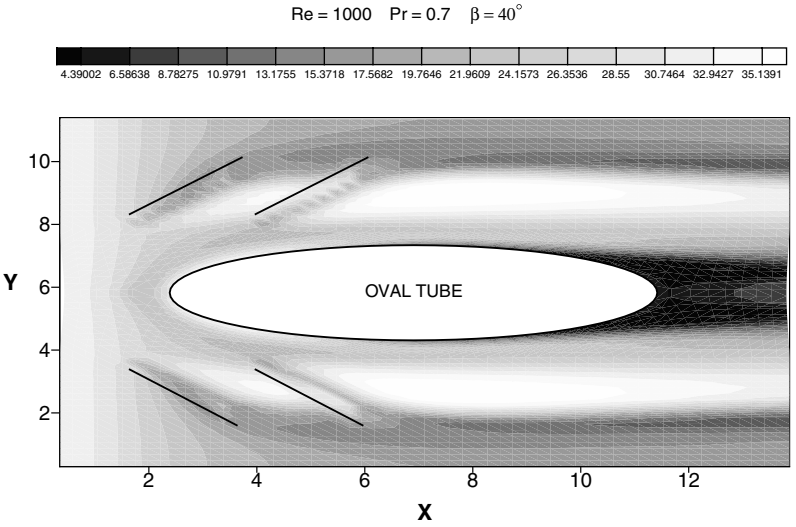

Fig. 10. Iso-Nusselt number distribution on the bottom plate for flow past a built-in oval tube with two winglet pairs (the configuration shown in Fig. 4(c)).

when compared to the previous case. For example, the region close to the wake zone and downstream to the winglet pairs is found to show improved heat transfer behavior in the latter configuration, although the region of enhanced heat transfer is greater in the former case.

Fig. 11 shows the iso-Nusselt number distribution on the bottom plate of the channel, for the parallel configuration of three winglet pairs (all W1, W2 and W3 in common-flow-down configuration as in Fig. 4(d)). The poor heat transfer associated with the wake zone is significantly reduced, and the zone of enhanced heat transfer gets appreciably broadened.

Fig. 12 shows the iso-Nusselt number distribution on the bottom plate of the channel for the configuration of four winglet pairs mounted simultaneously (W1 and W3 in common-flow-down configuration while W2 and W4 in common-flow-up configuration as in Fig. 4(e)). Here again the poor heat transfer associated with the wake zone is significantly reduced, and the zones of enhanced

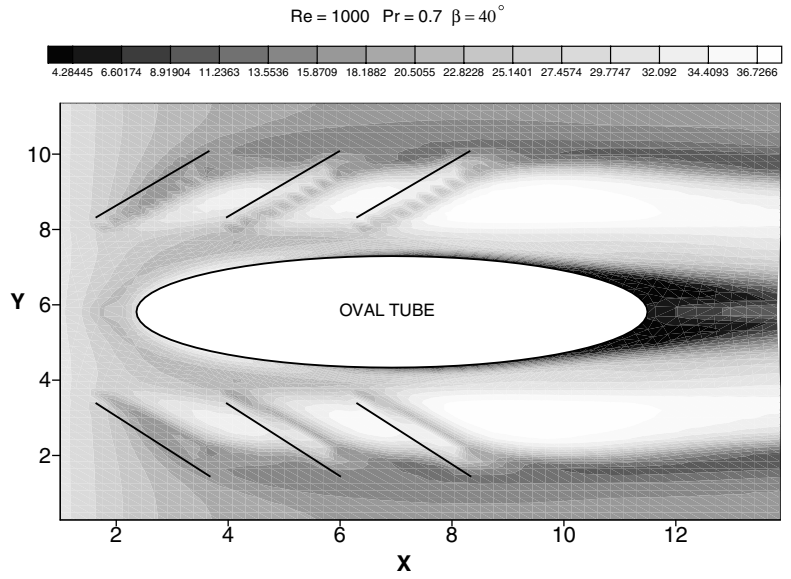

Fig. 11. Iso-Nusselt number distribution on the bottom plate for flow past a built-in oval tube with three winglet pairs (the configuration shown in Fig. 4(d)).

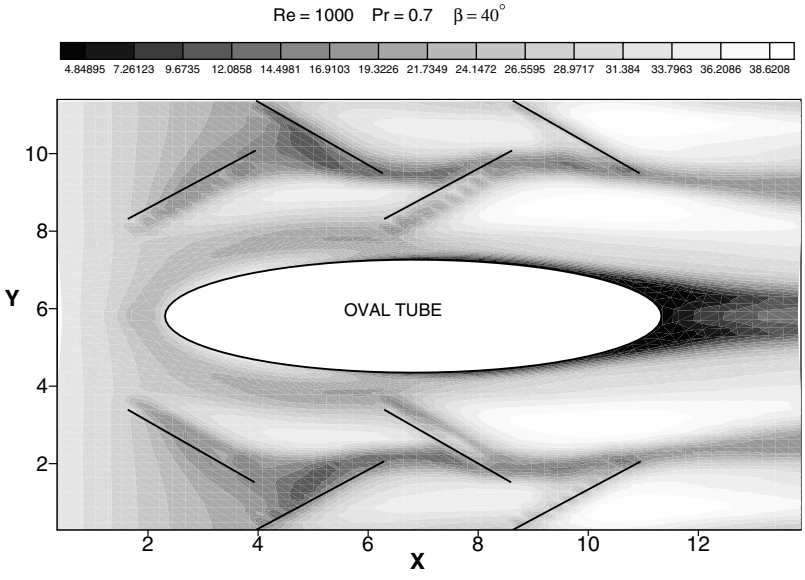

Fig. 12. Iso-Nusselt number distribution on the bottom plate for flow past a built-in oval tube with four winglet pairs (the configuration shown in Fig. 4(e)).

heat transfer get more broadly distributed in the spanwise direction.

Fig. 13 compares span-averaged Nusselt number distribution on the bottom wall of the channel, for the cases of (a) rectangular channel, (b) channel with built-in oval tube, (c) channel with built-in oval tube and one winglet pair (W1 in Fig. 4(a)) in common-flow-down configuration and (d) channel with built-in oval tube and two winglet pairs (both W1 and W2 in Fig. 4(a)), respectively in common-flow-down and common-flow-up configurations. The locations of the oval tube and winglets are also indicated at bottom of Fig. 3. For the case of a plane channel, the span-averaged Nusselt number decreases in downstream direction due to the

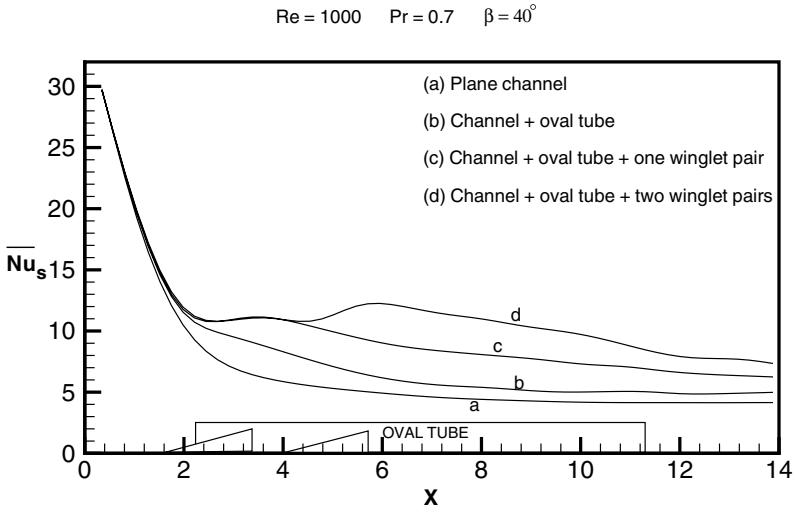

Fig. 13. Comparison of span-averaged Nusselt number for channel, channel with oval tube, channel with oval tube and one and two winglet pairs.

growth of the wall boundary layer and finally becomes almost constant (4.17) at the exit (curve marked as 'a'). With a built-in oval tube placed in the plane channel, there is an increase in the span-averaged Nusselt number at the axial location that corresponds to the forward stagnation zone (curve 'b'). This is due to the formation of horseshoe vortices in this zone. The value of the span-averaged Nusselt number at this location is 10.58. Curve 'c' shows the effect of winglet pair (W1) in common-flow-down configuration. At the axial location corresponding to the location of trailing edge of the winglet ($X = 3.61$), the span-averaged Nusselt number reaches a high value (11.18). The span-averaged Nusselt number is about 81% higher than that of a plane channel at the same axial location. Further improvement is shown when the two-winglet pairs (W1 and W2) are present simultaneously as indicated by curve 'd'. Here the maximum value of the span-averaged Nusselt number (12.22) is observed at the axial location corresponding to the location of the trailing edge of the second winglet pair (W2). This is at $X = 5.84$ with an enhancement of about 147% as compared to the span-averaged Nusselt number value for the plane channel at the same location. Table 1 compares the mean Nusselt number (global mean) for different obstacles used in this study. Percentage enhancement for the configuration of oval tube with winglets has been calculated by comparing it with the baseline case of a plane channel. We may also consider the oval tube as the essential part of the baseline configuration for a fin–tube heat-exchanger. On the basis of finned oval tube as the baseline case, the enhancement in last two configurations would become 24.16% and 43.86% respectively.

Table 1
Comparison of mean Nusselt number for different configurations

Configuration	Mean Nusselt number (global mean), Nu_m	% Nu_m enhancement
Plane channel	6.67	–
Channel with built-in oval tube	7.82	17.24
Channel with built-in oval tube and one winglet pair	9.71	45.58
Channel with built-in oval tube and two winglet pairs	11.25	68.66

Fig. 14 compares the span-averaged Nusselt number distribution in the channel with built-in oval tube and only one winglet pair (with $= 40°$), for various positions of one winglet pair (corresponding to the configuration in Fig. 4(a)). The mean Nusselt number (global mean), Nu_m is 9.71 for the location of the leading edge of the winglet pair at $X/L = 0.119$. Likewise, Nu_m is 9.22 for the location of leading edge of the winglet pair at $X/L = 0.186$, and it is 9.23 for $X/L = 0.254$. This shows that for better heat transfer the single winglet pair must be optimally mounted on the fin surface near the leading edge of the oval tube. The angle of attack, β was varied upto $\beta = 40°$, since there exists a possibility of vortex breakdown beyond $\beta = 45°$ (see [10]). Admittedly, the upper limit of $\beta = 40°$ is a conservative estimate. We have not tried the present simulation for $\beta > 40°$,

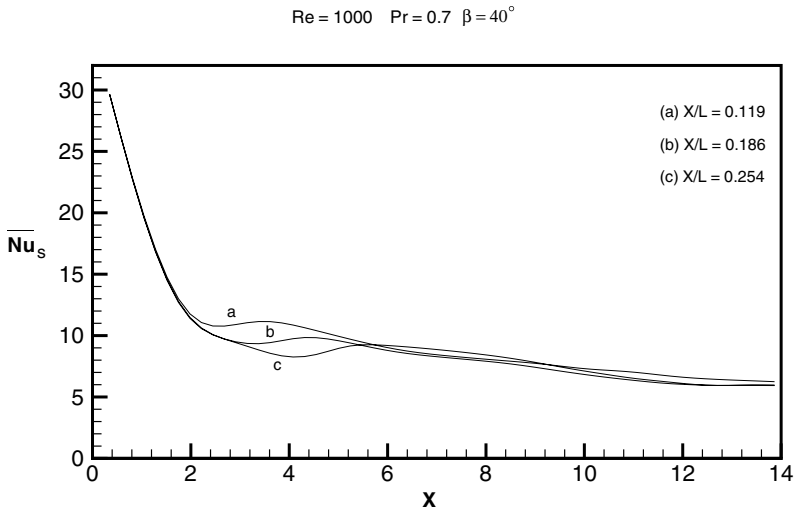

Fig. 14. Comparison of span-averaged Nusselt number for different axial locations of one winglet pair (the configuration shown in Fig. 4(a)).

though the Nusselt number, in similar applications, starts to decrease when β approaches 50°.

Fig. 15 compares the span-averaged Nusselt number distribution in the channel for the case of two winglet pairs mounted in staggered mode (the configuration shown in Fig. 4(b)) for different winglet angles of attack. The curves show similar qualitative trend but the winglet configuration with larger angle of attack shows higher value of span-averaged Nusselt number over a wide range. This is because winglets with larger angle of attack produce vortices of higher strength that result in better heat transfer. There always exists an optimum angle of attack beyond which 'vortex breakdown' may take place. That may destroy the desirable effect of the longitudinal vortices on heat transfer. Table 2 summarizes the effect of angle of attack on mean Nusselt number (global mean), Nu_m on the bottom plate of the channel. Table 3 shows the variation of average pressure drop in the duct, in the finned-oval-tube and in the duct with oval tube and winglets of varying orientation. The average pressure at any section was determined through the ratio of the area integral of pressure at that section

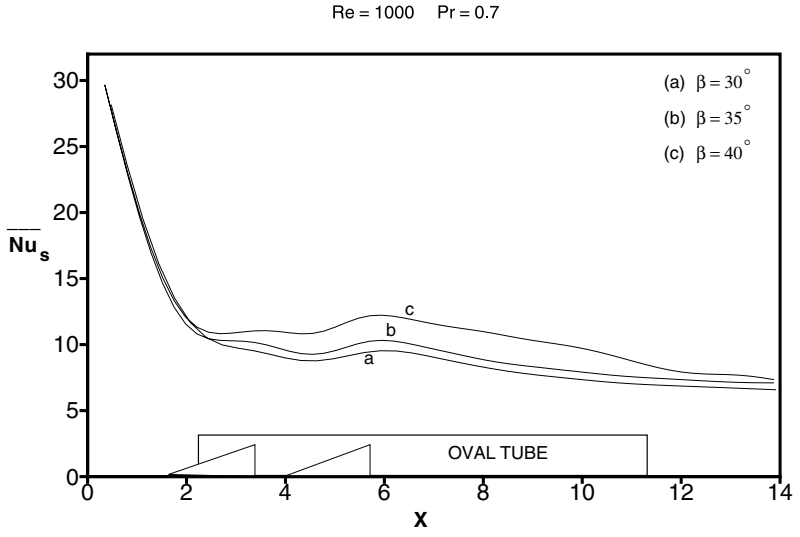

Fig. 15. Comparison of span-averaged Nusselt number for different angles of attack for flow past a built-in oval tube with two winglet pairs (the configuration shown in Fig. 4(b)).

Table 2
Comparison of Mean Nusselt number for different angles of attack

Configuration	Mean Nusselt number (global mean), Nu_m	% Nu_m enhancement
Without winglet pairs	7.82	–
$\beta = 30$	9.37	19.82
$\beta = 35$	10.00	27.88
$\beta = 40$	11.25	13.86

Table 3
Pressure drop in the duct for various configurations

Configuration	$(\Delta p) \times Re$	% increase in $\Delta p \times Re$
Plane channel	870.57	–
Channel with built-in oval tube	1467.86	68.61
Channel with built-in oval tube and one winglet pair	1508.23	73.31
Channel with built-in oval tube and two winglet pairs	1586.60	82.25

to the cross-sectional area. The dimensionless pressure drop in Table 3 has been scaled with the Reynolds number entailing the matching points at the entry plane of the channel. On the basis of a plane channel as the baseline case, the additional pressure penalty for the subsequent configurations are 68.61%, 73.31% and 82.25% respectively.

Fig. 16 compares the variation of span-averaged Nusselt number corresponding to the parallel configurations of one, two and three pairs of winglets (configured as in Fig. 4(a), (c) and (d)). Here each extra-added pair of the winglet is in common-flow-up configuration and can be seen to enhance the heat transfer effectively, especially in the dead water zone. The only constraint of adding extra pair of winglets to enhance heat transfer appears in terms of controlling the pressure loss penalty. The enhanced heat transfer is almost of the order of 100% near the dead water zone in the present case, as compared to the flow past an oval tube in absence of winglet pairs.

Fig. 17 compares the span-averaged Nusselt number corresponding to the winglet configurations shown in Fig. 4(b) and (e). Here the first case has a staggered arrangement of two pairs of winglets (W1 and W2 in common-flow-down and common-flow-up configurations respectively) and the second one has two such arrangements one after the other along the length. In both the cases, the variations of span-averaged Nusselt number from channel inlet till the end location of W2 (Fig. 4(e)) is same, but there is strong increase in the value of $\overline{Nu_s}$ beyond this location for the second case. There is an increment in heat transfer to the extent of nearly 180% in the dead water zone, as compared to the case of flow past an oval tube in absence of winglet pairs.

Fig. 18 shows the variation of span-averaged Nusselt number in the flow direction for three different Reynolds numbers, $Re = 500$, 1000 and 1500 with one pair of winglet mounted in common-flow-down configuration. An increase in $\overline{Nu_s}$ is observed all along the channel length with increasing value of the Reynolds number.

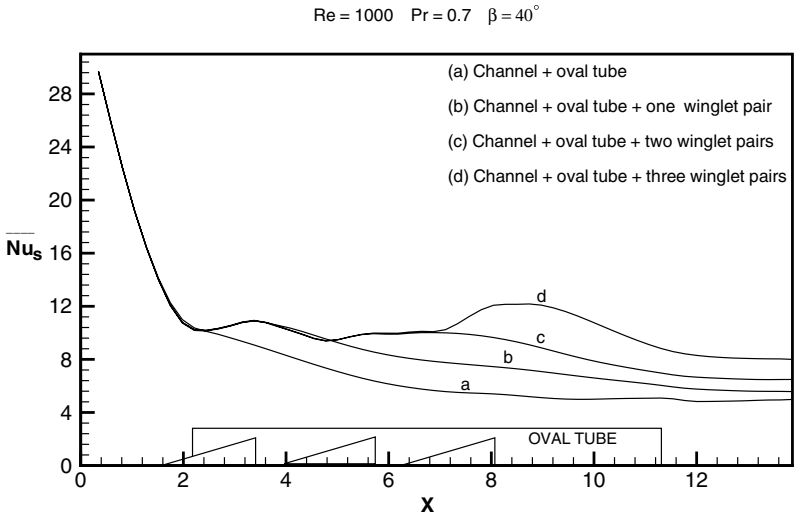

Fig. 16. Comparison of span-averaged Nusselt number for flow past a built-in oval tube with one, two and three winglet pairs (the configurations in Fig. 4(a), (c) and (d) respectively).

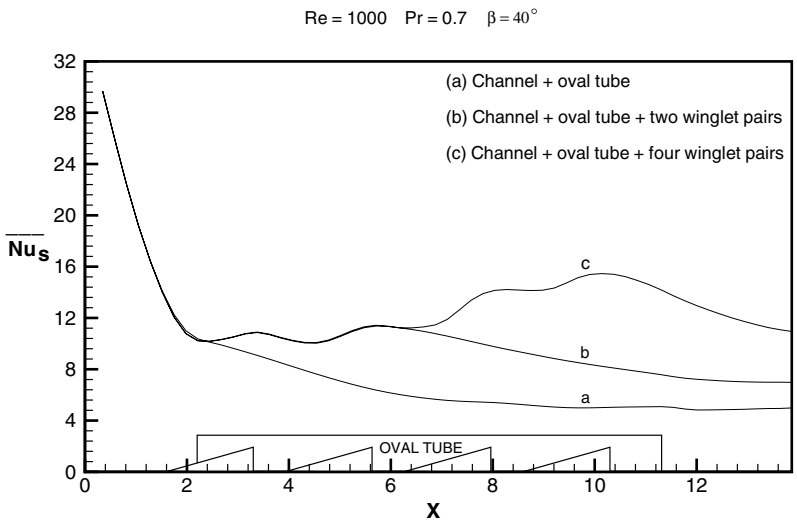

Fig. 17. Comparison of span-averaged Nusselt number for flow past a built-in oval tube with two and four winglet pairs (the configurations in Fig. 4(b) and (e) respectively).

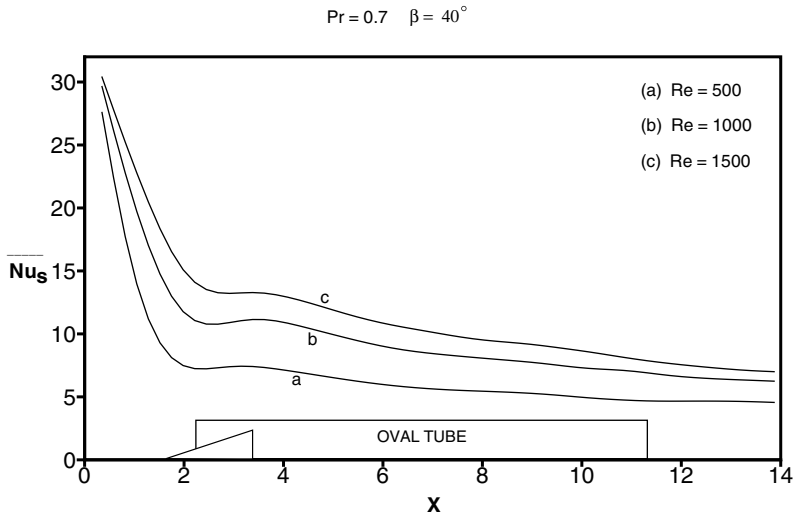

Fig. 18. Comparison of span-averaged Nusselt number for different Reynolds numbers for flow past a built-in oval tube with one winglet pair (the configuration show in Fig. 4(a)).

This may be expected due to the following reason. At higher value of Reynolds number, the thermal boundary layer thickness decreases and the degree of fluid mixing increases. As a consequence, a global enhancement in heat transfer is observed with increasing values of Reynolds number.

Fig. 19 compares the span-averaged Nusselt number distribution on the bottom wall of the channel for three different grids for the flow through a channel with built-in oval tube and one winglet pair in common-flow-down configuration (Fig. 4(a)). Three different grid-meshes, namely, $62 \times 61 \times 19$, $72 \times 71 \times 21$ and $82 \times 81 \times 25$ were utilized to test the grid sensitivity. The results reveal minor changes (less than 4%) in span-averaged value of Nusselt number, at any axial location in the channel, for the three different grids.

Fig. 20 compares the experimentally obtained span-averaged Nusselt number distribution based on the inlet fluid temperature [11] with the computed span-averaged Nusselt number distribution for the finned oval tube with constant fin temperature. In the experimental study, the Nusselt numbers are deduced from the heat

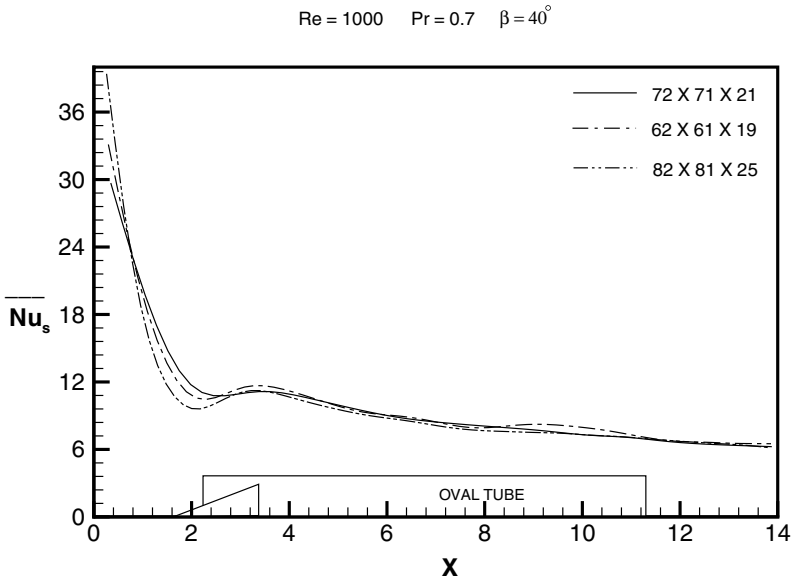

Fig. 19. Comparison of span-averaged Nusselt number for three different grid sizes (the configuration shown in Fig. 4(a)).

and mass transfer analogy. The ammonia absorption measurements (AAM) were performed on a finned oval tube model in a wind tunnel for a Reynolds number of 1090 [11]. Starting from the location $X = 4$, the measured and computed results agree quite well, but there exists some discrepancy in the earlier part from $X = 0$ to 4. The reason for this discrepancy may be due to differences of the velocity distribution at the entrance in the experimental and numerical studies. For the present computation, a uniform velocity distribution was employed at the inlet, while in the experiment, it would be difficult to realize a uniform velocity at the inlet. Besides, the measurement of the high mass transfer at the leading edge by the ammonia absorption technique is very likely to be error prone [11].

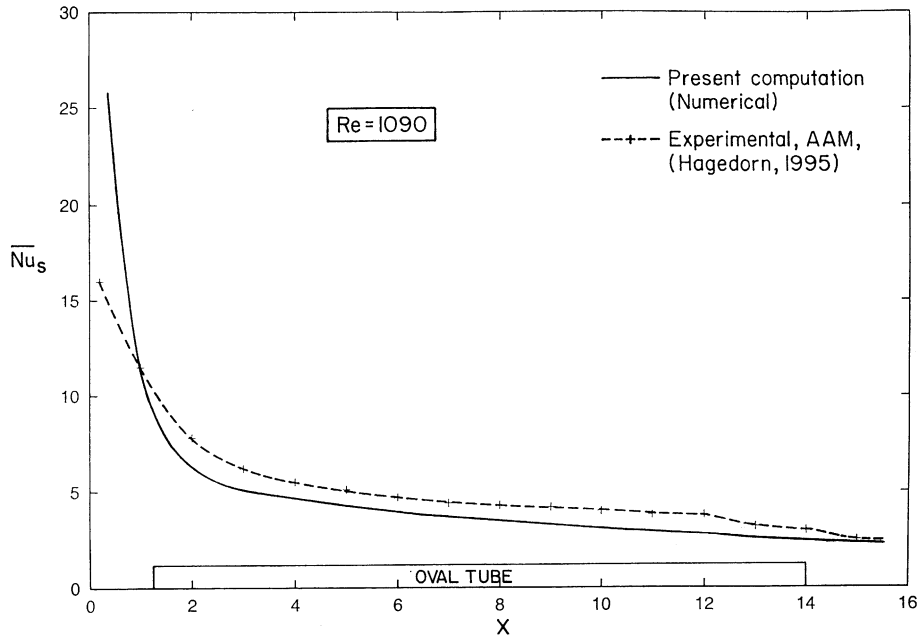

Fig. 20. Comparison of experiment and numerical span-averaged Nusselt number for $Re = 1090$.

8. Conclusions

A three-dimensional computational study of forced convection heat transfer has been accomplished to determine the flow structure and heat transfer in a rectangular channel with a built-in oval tube and delta-winglet type vortex generators in various configurations. The duct was designed to simulate a passage, formed by two neighboring fins in a fin–tube heat exchanger. The present study reveals that combinations of oval tube and the winglet pairs improve the heat transfer significantly, especially in the dead water zone. The mean span-averaged Nusselt number for the case of four winglet pairs, each two in sequence having a staggered configuration (inner pair in common-flow-down and outer pair in common-flow-up arrangement) is about 100% higher as compared to no-winglet case at a Reynolds number of 1000. The enhancement in heat transfer, on the basis of finned oval tube as the base line case, is 43.86% for the case of two winglet pairs in staggered mode. A comparison of heat transfer for the cases of one, two and three winglet pairs (all in common-flow-down configuration) confirms that the addition of each extra winglet pair causes further enhancement of heat transfer. The enhancement of heat transfer is marked even at far downstream locations. The winglets, at their moderate angle of attack, have quite streamlined like behavior and so, are not expected to contribute much towards pressure losses. On the other hand, the contribution towards enhancement in heat transfer due to the winglet pairs is undoubtedly significant.

Acknowledgements

This investigation has been sponsored by the New Energy and Industrial Development Organization (NEDO), Japan.

References

[1] G. Biswas, N.K. Mitra, M. Fiebig, Heat transfer enhancement in fin–tube heat exchangers by winglet-type vortex generators, Int. J. Heat Mass Transfer 37 (1994) 283–291.
[2] A. Valencia, M. Fiebig, N.K. Mitra, Heat transfer enhancement by longitudinal vortices in fin–tube heat exchanger element with flat tubes, J. Heat Transfer (ASME) 118 (1996) 209–211.
[3] J.E. O'Brien, M.S. Sohal, Local heat transfer for finned-tube heat exchangers using oval tubes, Proceedings of NHTC'00, 34th National Heat Transfer Conference Pittsburgh, Pennsylvania, USA, 2000.
[4] W.R. Pauley, J.K. Eaton, Experimental study of the development of longitudinal vortex pairs embedded in a turbulent boundary layer, AIAA J. 26 (1988) 816–823.
[5] S. Kakac, R.K. Shah, A.E. Bergles, Low Reynolds number flow heat exchangers, Hemisphere, Washington DC, USA, 1981.
[6] I. Orlanski, A simple boundary condition for unbounded flows, J. Comput. Phys. 21 (1976) 251–269.
[7] V. Eswaran, S. Prakash, A finite volume method for Navier–Stokes equations, Proceedings of the third Asian CFD Conference, Bangalore, vol. 1, 1998, pp. 251–269.
[8] V. Prabhakar, G. Biswas, V. Eswaran, Numerical prediction of heat transfer in a channel with a built-in oval tube and two different shaped vortex generators, Numer. Heat Transfer Part A 41 (2002) 307–329.
[9] G. Biswas, K. Tori, D. Fujii, K. Nishino, Numerical and experimental determination of flow structure and heat transfer effects of longitudinal vortices in a channel flow, Int. J. Heat Mass Transfer 39 (16) (1996) 3441–3451.
[10] G. Biswas, N.K. Mitra, Longitudinal vortex generators for enhancement of heat transfer in heat exchanger applications, Proceedings of 11th IHTC, Kyongju, Korea, vol. 5, 1998, pp. 339–344.
[11] M. Hagedorn, Untersuchung des Wärmerberganges und des Strömungsverlustes an lamellen Rohr Wärmerbertragermodulen unter Berücksichtigung der Wärmeleitung in den Lamellen, Diplomerbeit Nr. 95-07, Institut Für Thermo-und Fluiddynamik, Ruhr-Universität Bochum, Germany, 1995.